Majorana differential shot noise and its universal thermoelectric crossover

Sergey Smirnov *

P. N. Lebedev Physical Institute of the Russian Academy of Sciences, 119991 Moscow, Russia

(Received 14 December 2022; revised 22 February 2023; accepted 3 April 2023; published 11 April 2023)

Nonequilibrium states driven by both electric bias voltages V and temperature differences ΔT (or thermal voltages $eV_T \equiv k_B \Delta T$) are unique probes of various systems. Whereas average currents $I(V, V_T)$ are traditionally measured in majority of experiments, an essential part of nonequilibrium dynamics, stored particularly in fluctuations, remains largely unexplored. Here we focus on Majorana quantum dot devices, specifically on their differential shot noise $\partial S^{>}(V, V_T)/\partial V$, and demonstrate that in contrast to the differential electric or thermoelectric conductance, $\partial I(V, V_T)/\partial V$ or $\partial I(V, V_T)/\partial V_T$, it reveals a crossover from thermoelectric to pure thermal nonequilibrium behavior. It is shown that this Majorana crossover in $\partial S^{>}(V, V_T)/\partial V$ is induced by an interplay of the electric and thermal driving, occurs at an energy scale determined by the Majorana tunneling amplitude, and exhibits a number of universal characteristics which may be accessed in solely noise experiments or in combination with measurements of average currents.

DOI: 10.1103/PhysRevB.107.155416

I. INTRODUCTION

Topological superconductors interacting with nanoscopic setups provide a feasible technological platform to entangle a specific quantum core of these setups with non-Abelian Majorana bound states (MBSs) [1–7] imitating particle-antiparticle paradigm of the Abelian Majorana fermions [8] known in the particle physics. Such Majorana entangled setups are understood (without a strict relation to the specific meaning of "entanglement" in quantum information) as those where Majorana and non-Majorana degrees of freedom are coupled via a certain quantum mechanical mechanism. They represent a special class of condensed matter systems which are very attractive both from theoretical and experimental perspectives. On one side, they admit an observation of diverse physical phenomena governed essentially by Majorana entangled states and, on the other side, they may function as elementary blocks integrated in various fault tolerant topological quantum computing [9] schemes designed to process the quantum nonlocality supported by MBSs.

Nanoscopic setups where MBSs are entangled with the quantum degrees of freedom involved in experimental measurements reveal various remarkable characteristics many of which may be accessed in quantum transport experiments. Such experiments deal with nonequilibrium states which may be generated by bias voltages V or temperature differences ΔT, expressed equivalently through the corresponding thermal voltages V_T, defined as $eV_T \equiv k_B \Delta T$. Here Majorana features are predicted within the framework of mean currents $I(V)$ induced by mostly bias voltages [10–36] or, to a lesser extent, mean currents $I(V, V_T)$ induced by also temperature differences [37–47]. Experimental efforts on mean currents $I(V)$ induced by bias voltages [48–50] are aimed to measure the differential conductance $\partial I(V)/\partial V$. Of particular interest here is the zero bias limit of the differential conductance (linear conductance) which should attain a certain universal value predicted theoretically for a specific Majorana entangled setup. Although such mean current experiments are well developed and should be performed in the first place, unfortunately, they may be controversial [51,52] in detecting MBSs and, as a consequence, other types of quantum transport measurements, or perhaps sequences of measurements [53], are currently in demand. Particularly, one is interested in those physical observables which demonstrate in a given setup a Majorana driven behavior which is qualitatively different from the behavior of the mean currents measured in the same Majorana entangled setup.

An attractive quantum transport alternative to the mean value of a current flowing through a nanoscopic setup is to study the random deviations of this current from its mean value, that is the current fluctuations, characterized, for example, by the shot noise $S^{>}$. Here the majority of Majorana shot noise proposals assume nonequilibrium states originating from bias voltages [54–64] and explore the behavior of $S^{>}(V)$ at small and large V. As in mean current experiments, where the differential conductance $\partial I(V)/\partial V$ provides an access to an averaged Majorana universality, the differential shot noise $\partial S^{>}(V)/\partial V$ allows one to reveal a universal fluctuation behavior governed by Majorana entangled states.

One may also avoid resorting to nonequilibrium behavior and address Majorana entangled states in corresponding equilibrium nanoscopic setups by means of quantum thermodynamic tools such as the entropy of these setups [65–69]. Recent experimental and theoretical activities [70–76] on the entropy of nanoscale and mesoscale systems demonstrate that this engrossing approach may become a powerful and univocal technique which will not be subject to further controversy similar to the one about the Majorana differential conductance.

*sergej.physik@gmail.com;
sergey.smirnov@physik.uni-regensburg.de;
ssmirnov@sci.lebedev.ru

Nevertheless, presently quantum transport is a more appealing framework within which experimentalists have at their disposal well established technologies verified in diverse nanoscopic setups for a long period of time. Moreover, quantum transport techniques have a wider space of control due to numerous additional parameters utilized to maintain various kinds of nonequilibrium states in which a broad spectrum of physical observables is available for performing experiments. Thus applying the quantum transport framework to Majorana entangled nanoscopic setups provides vast freedom in exploring Majorana phenomena in nonequilibrium. In particular, among measurements of other physical observables, shot noise experiments in various nonequilibrium states are expected to qualitatively enrich the existing results on mean currents in Majorana entangled nanoscopic setups.

Here we focus on the shot noise in nonequilibrium states produced by bias voltages V and thermal voltages V_T in a quantum dot (QD) whose degrees of freedom are entangled with MBSs of a topological superconductor. Specifically, we explore the differential shot noise $\partial S^{>}(V,V_T)/\partial V$ which, as has been discussed above, inspects universal Majorana fluctuation behavior. So far, not much is known about this physical observable when both V and V_T excite competing current flows in a Majorana setup. Indeed, whereas the differential thermoelectric shot and quantum noise, $\partial S^{>}(V,V_T)/\partial V_T$, have been addressed [77,78] in the presence of both bias voltages and temperature differences, the differential shot noise $\partial S^{>}(V,V_T)/\partial V$ remains to a large extent unexplored for Majorana entangled setups in nonequilibrium states driven by both V and V_T. It should be noted that in nonequilibrium states induced only by bias voltages V the differential shot noise has been studied in combination with the differential conductance. In particular, in Ref. [79] it is demonstrated that in the presence of MBSs a dip of the differential shot noise is always accompanied by a peak of the differential conductance. This behavior has also been observed earlier in Ref. [64] (see its Fig. 4, namely, the insets of the upper panel). As mentioned above, it is important to find for a given Majorana entangled setup physical observables whose behavior has a character qualitatively different from the one of the mean current or its derivative physical quantities such as the differential conductance $\partial I(V,V_T)/\partial V$ or differential thermoelectric conductance $\partial I(V,V_T)/\partial V_T$ whose behavior may be obtained in the same setup. We demonstrate that the differential shot noise is one of such physical observables which is distinguished by the presence of a crossover from a thermoelectric to pure thermal nonequilibrium behavior. It is shown that whereas the differential shot noise passes through its crossover, the differential conductance and differential thermoelectric conductance do not exhibit any crossover or any other peculiarity. Thus, in contrast to $\partial I(V,V_T)/\partial V$ and $\partial I(V,V_T)/\partial V_T$, the differential shot noise $\partial S^{>}(V,V_T)/\partial V$ brings a nonequilibrium energy scale having a pure fluctuation nature meaning that it cannot be revealed within measurements limited only by the mean current. Besides being of fundamental interest, the energy scale associated with the nonequilibrium crossover in $\partial S^{>}(V,V_T)/\partial V$ is shown to be of practical importance in expressing quantitatively the fluctuation universality of Majorana entangled states via a number of measurable universal ratios which would be of interest for future experiments.

The paper is organized as follows. In Sec. II we discuss a theoretical model of an experimentally feasible nanoscopic setup where MBSs are entangled with a QD whose nonequilibrium states are generated by both a bias voltage and thermal voltage. Results of numerical analysis performed with high accuracy for the differential shot noise $\partial S^{>}(V,V_T)/\partial V$, differential conductance $\partial I(V,V_T)/\partial V$, and differential thermoelectric conductance $\partial I(V,V_T)/\partial V_T$ are presented in Sec. III where it is demonstrated that, in contrast to $\partial I(V,V_T)/\partial V$ and $\partial I(V,V_T)/\partial V_T$, one observes in $\partial S^{>}(V,V_T)/\partial V$ a crossover from a thermoelectric to pure thermal nonequilibrium behavior. The energy scale where this crossover takes place and a number of universal Majorana ratios involving this energy scale are also shown in this section. Finally, with Sec. IV we make conclusions and discuss possible outlooks.

II. THEORETICAL MODEL OF A MAJORANA ENTANGLED QUANTUM DOT AND THE DIFFERENTIAL SHOT NOISE IN THERMOELECTRIC NONEQUILIBRIUM

We start with a description of a setup which, on one side, is technologically feasible [80,81] and, on the other side, involves a basic mechanism of a Majorana entanglement which is sufficient to demonstrate a remarkable nonequilibrium behavior of the differential shot noise in presence of both bias voltages and temperature differences. To this end, let us consider a noninteracting QD,

$$\hat{H}_{\rm QD}=\epsilon_d d^\dagger d. \tag{1}$$

The QD is nondegenerate and its energy level ϵ_d is tunable by a proper gate voltage. The choice of a setup with a noninteracting QD is quite a realistic assumption to explore universal Majorana phenomena at low energies. Indeed, the spin degeneracy is assumed to be removed by an external magnetic field which excludes a possible interfering of an interaction induced Kondo universal behavior, well-known in experiment and theory of spin-degenerate QDs [82–88], with the low-energy Majorana universal effects, which are of interest in this work. Numerical renormalization group calculations [89] have demonstrated that interacting spin-degenerate QDs in external magnetic fields behave similar to noninteracting nondegenerate QDs exhibiting, for example, the linear conductance $e^2/2h$ which results entirely from the Majorana entangled states. Thus Eq. (1) is a proper model to explore low-energy Majorana quantum transport, in particular, in nonequilibrium states resulting from bias voltages and temperature differences [38].

Two normal noninteracting metallic contacts, denoted below as left (L) and right (R),

$$\hat{H}_C=\sum_{l=\{L,R\}}\sum_k \epsilon_k c_{lk}^\dagger c_{lk}, \tag{2}$$

are connected to the QD via tunneling processes,

$$\hat{H}_{{\rm QD}-C}=\sum_{l=\{L,R\}}\mathcal{T}_l\sum_k c_{lk}^\dagger d+{\rm H.c.} \tag{3}$$

In Eq. (2) the continuous energy spectrum ϵ_k gives rise to a density of states of the contacts $\nu_C(\epsilon)$ which is in general energy dependent. However, around the Fermi energy one (usually with a good accuracy) assumes that its energy dependence plays no essential role for quantum transport and thus $\nu_C(\epsilon) \approx \nu_0/2$. In Eq. (3) one additionally assumes that the tunneling matrix elements do not depend on the set k of the quantum numbers used to describe the states in the contacts, $\mathcal{T}_{kl} \approx \mathcal{T}_l$. The relevant energy scales brought about by the tunneling between the QD and contacts are $\Gamma_l = \pi\nu_0|\mathcal{T}_l|^2$. By proper gate voltages one may achieve the symmetric coupling $\Gamma_L = \Gamma_R = \Gamma/2$ which will be assumed below.

Each contact is assumed to be in its own equilibrium state with the corresponding Fermi-Dirac distribution,

$$f_l(\epsilon) = \frac{1}{\exp\left(\frac{\epsilon-\mu_l}{k_B T_l}\right)+1}. \tag{4}$$

Here the chemical potentials,

$$\mu_{L,R} = \mu_0 \pm eV/2, \tag{5}$$

are specified by the bias voltage V such that $eV < 0$ and the temperature of the left contact is higher than the temperature of the right contact, that is

$$\begin{aligned} T_L &= T + \Delta T \quad \text{(hot contact)}, \\ T_R &= T \quad \text{(cold contact)}, \end{aligned} \tag{6}$$

assuming $T, \Delta T \geqslant 0$. The QD is out of equilibrium when either $V \neq 0$ or $\Delta T \neq 0$.

A topological superconductor hosting two MBSs $\gamma_{1,2}$ at its ends,

$$\hat{H}_{TS} = \tfrac{1}{2} i\xi\gamma_2\gamma_1, \quad \gamma_{1,2}^\dagger = \gamma_{1,2}, \quad \{\gamma_i, \gamma_j\} = 2\delta_{ij}, \tag{7}$$

interacts with the QD,

$$\hat{H}_{\text{QD}-TS} = \eta^* d^\dagger \gamma_1 + \text{H.c.}, \tag{8}$$

implementing a direct entanglement of the QD's degrees of freedom with the Majorana mode γ_1 of the topological superconductor. In Eq. (7) the parameter ξ is an energetic measure of how strong the two Majorana modes overlap with each other. When ξ is small the MBSs are well separated whereas large values of ξ model a situation where the two MBSs merge into a single Dirac fermion. In Eq. (8) the Majorana tunneling amplitude $|\eta|$ specifies the strength of the Majorana entanglement.

A schematic summary of the above theoretical formulation of the setup, based on Eqs. (1)–(8), is illustrated in the inset of Fig. 1.

The Hamiltonian of the setup, $\hat{H} = \hat{H}_{\text{QD}} + \hat{H}_C + \hat{H}_{\text{QD}-C} + \hat{H}_{TS} + \hat{H}_{\text{QD}-TS}$, allows us to formulate the problem in terms of the Keldysh field integral [90], a convenient tool to calculate various correlation functions. Other technical tools based, e.g., on quantum master equations [91] may also be considered as alternative approaches to the problem. Within the Keldysh field integral formalism one may straightforwardly derive the shot noise from the Keldysh generating functional,

$$Z[J_{lq}(t)] = \int \mathcal{D}[\bar{\psi}, \psi; \bar{\phi}, \phi; \bar{\zeta}, \zeta] e^{\frac{i}{\hbar} S_K[J_{lq}(t)]}, \tag{9}$$

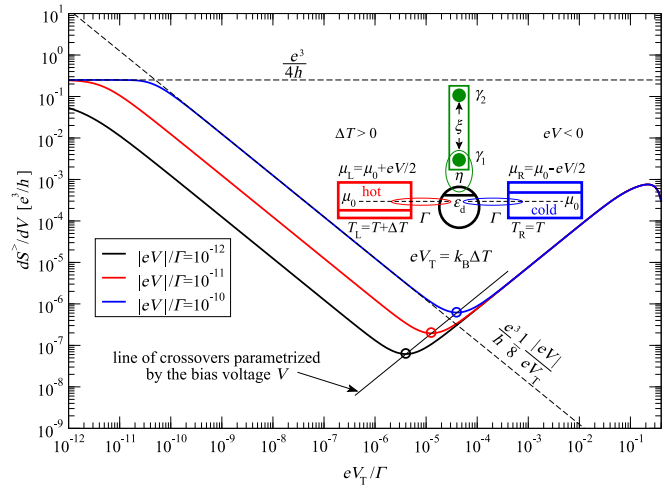

FIG. 1. Differential shot noise $\partial S^>/\partial V$ as a function of the thermal voltage V_T for three different values of the bias voltage: $|eV|/\Gamma = 10^{-12}$ (black), $|eV|/\Gamma = 10^{-11}$ (red), $|eV|/\Gamma = 10^{-10}$ (blue). The other parameters have the following values: $\epsilon_d/\Gamma = 10^{-1}$, $k_BT/\Gamma = 10^{-12}$, $|\eta|/\Gamma = 1$, $\xi/\Gamma = 10^{-14}$. The Majorana device presented above the curves illustrates schematically the physical setup, described in the main text, Eqs. (1)–(8), assuming $eV < 0$ and $\Delta T > 0$.

which is a field integral over the Grassmann fields of the QD ($\bar{\psi}_q(t), \psi_q(t)$), contacts ($\bar{\phi}_{lkq}(t), \phi_{lkq}(t)$) and topological superconductor ($\bar{\zeta}_q(t), \zeta_q(t)$) whose temporal arguments are on the real axis and $q = \pm$ specifies, respectively, the forward or backward branch of the Keldysh contour. At zero source fields the Keldysh generating functional is determined by the Keldysh action $S_K^{(0)} \equiv S_K[J_{lq}(t) = 0]$ and is equal to unity, $Z[J_{lq}(t) = 0] = 1$. The Keldysh action $S_K[J_{lq}(t)]$,

$$\begin{aligned} S_K[J_{lq}(t)] = {} & S_{\text{QD}}[\bar{\psi}, \psi] + S_C[\bar{\phi}, \phi] + S_{TS}[\bar{\zeta}, \zeta] \\ & + S_{\text{QD}-C}[\bar{\psi}, \psi; \bar{\phi}, \phi] + S_{\text{QD}-TS}[\bar{\psi}, \psi; \bar{\zeta}, \zeta] \\ & + S_O[\bar{\psi}, \psi; \bar{\phi}, \phi; J_{lq}(t)], \end{aligned} \tag{10}$$

is the sum of, respectively, the actions describing the QD, contacts, topological superconductor, tunneling between the QD and contacts, tunneling between the QD and topological superconductor and the source action added to generate an observable of interest, in particular, the mean current and shot noise. The actions S_{QD}, S_C, and S_{TS} are of the standard matrix form [90] in the retarded-advanced space. The actions $S_{\text{QD}-C}$, $S_{\text{QD}-TS}$, and S_O have the following form:

$$S_{\text{QD}-C} = -\int_{-\infty}^{\infty} dt \sum_{l=\{L,R\}} \sum_{k,q} [\mathcal{T}_l q \bar{\phi}_{lkq}(t)\psi_q(t) + \text{G.c.}], \tag{11}$$

$$\begin{aligned} S_{\text{QD}-TS} = -\int_{-\infty}^{\infty} dt \Big\{ & \eta^* \sum_q q[\bar{\psi}_q(t)\zeta_q(t) \\ & + \bar{\psi}_q(t)\bar{\zeta}_q(t)] + \text{G.c.} \Big\}, \end{aligned} \tag{12}$$

$$S_O = -\int_{-\infty}^{\infty} dt \sum_{l=\{L,R\}} \sum_q J_{lq}(t) I_{lq}(t), \tag{13}$$

where G.c. denotes the Grassmann conjugated terms and $I_{lq}(t)$ is the current operator in the Grassmann representation,

$$I_{lq}(t) = \frac{ie}{\hbar}\sum_k (\mathcal{T}_l \bar{\phi}_{lkq}(t)\psi_q(t) - \text{G.c.}). \tag{14}$$

The form of the source action in Eq. (13) implies that one derives the mean current and current-current correlations via proper differentiations,

$$\langle I_{lq}(t)\rangle_0 = i\hbar \frac{\delta Z[J_{lq}(t)]}{\delta J_{lq}(t)}\bigg|_{J_{lq}(t)=0}, \tag{15}$$

$$\langle I_{lq}(t) I_{l'q'}(t')\rangle_0 = (i\hbar)^2 \frac{\delta^2 Z[J_{lq}(t)]}{\delta J_{lq}(t)\delta J_{l'q'}(t')}\bigg|_{J_{lq}(t)=0}, \tag{16}$$

where

$$\left\langle \prod_i I_{l_i q_i}(t_i)\right\rangle_0 \equiv \int \mathcal{D}[\bar{\psi},\psi;\bar{\phi},\phi;\bar{\xi},\xi] e^{\frac{i}{\hbar}S_K^{(0)}} \prod_i I_{l_i q_i}(t_i). \tag{17}$$

Choosing the left contact as the one where measurements of the mean current

$$I(V,V_T) = \langle I_{Lq}(t)\rangle_0, \tag{18}$$

and correlations

$$S^>(t,t';V,V_T) = \langle \delta I_{L-}(t)\delta I_{L+}(t')\rangle_0 \tag{19}$$

of the current fluctuations

$$\delta I_{Lq}(t) = I_{Lq}(t) - I(V,V_T) \tag{20}$$

are performed, one obtains the shot noise $S^>(V,V_T)$ in the left contact as the zero frequency Fourier transform of $S^>(t,t';V,V_T) = S^>(t-t';V,V_T)$,

$$S^>(\omega;V,V_T) = \int_{-\infty}^{\infty} dt\, e^{i\omega t} S^>(t;V,V_T),$$
$$S^>(V,V_T) = S^>(\omega=0;V,V_T). \tag{21}$$

As it has already been mentioned in Sec. I, the majority of quantum transport experiments deal with mean currents, Eq. (18), specifically, with their differential characteristics such as the differential conductance or, less often, differential thermoelectric conductance, $\partial I(V,V_T)/\partial V$ or $\partial I(V,V_T)/\partial V_T$, respectively. These quantities have universal units of e^2/h and thus provide direct access to universal properties of MBSs. Likewise, experiments dealing with shot noises, Eq. (21), and their derivatives, may access universal fluctuation behavior of Majorana entangled states via, for example, the differential shot noise, $\partial S^>(V,V_T)/\partial V$, having universal units of e^3/h. Whereas the Majorana universality of $\partial S^>/\partial V$ is still an experimental challenge for Majorana entangled setups, the differential shot noise has already been successfully measured to probe other types of fluctuation universality, for example the universality of the Kondo noise in quantum dots [92]. Although experiments on current fluctuations are more complicated than those measuring mean currents, the results of such noise measurements provide a much more detailed microscopic structure of various nanoscopic setups.

Below we obtain the differential conductance $\partial I(V,V_T)/\partial V$, differential thermoelectric conductance $\partial I(V,V_T)/\partial V_T$, and differential shot noise $\partial S^>(V,V_T)/\partial V$ by means of numerical calculations based on finite differences used to approximate the corresponding derivatives. Here we would like to emphasize that although the above theoretical model is noninteracting, numerical calculations of $S^>(V,V_T)$ and $I(V,V_T)$ are nevertheless necessary. The point is that after obtaining closed analytic expressions for $S^>(V,V_T)$ and $I(V,V_T)$, which is possible because the Keldysh field integral is quadratic in the fermionic fields, it still remains to perform integrals in the energy domain (see the Appendix in Ref. [77]) in these analytic expressions. These integrals are hard to calculate analytically, especially, at finite temperature differences (characterized by finite thermal voltages V_T), that is when the Fermi-Dirac distributions in Eq. (4) cannot be approximated by steplike functions. In general, calculations of the differential shot noise are more time consuming than those which would be necessary to get just the shot noise. Whereas a certain numerical accuracy may be sufficient to get curves looking smooth enough for $S^>(V,V_T)$, using the same numerical data to calculate $\partial S^>(V,V_T)/\partial V$ may result in numerical errors leading to a chaotic data set. Thus to obtain $\partial S^>(V,V_T)/\partial V$ with an accuracy that allows one to identify dependence on various parameters as well as corresponding coefficients, the calculation of $S^>(V,V_T)$ should be done with a proper precision. Clearly, a higher degree of numerical accuracy leads to a notable increase of the computational time but still makes it possible to perform for the setup described in this section a detailed analysis of $\partial S^>(V,V_T)/\partial V$, in particular, its universal Majorana thermoelectric crossover discussed thoroughly in the next section.

III. NUMERICAL ANALYSIS OF THE DIFFERENTIAL SHOT NOISE AND ITS THERMOELECTRIC CROSSOVER

In this section we present numerical results for the differential shot noise $\partial S^>(V,V_T)/\partial V$ and demonstrate that, in contrast to the differential conductance $\partial I(V,V_T)/\partial V$ and differential thermoelectric conductance $\partial I(V,V_T)/\partial V_T$, it exhibits a crossover from one type of nonequilibrium behavior to a qualitatively different one. This crossover occurs in the regime

$$\Gamma \gg eV_T \gg |eV| \gg \xi, \tag{22}$$

and in the most part of this section we focus on quantum transport in this regime except for the last part where we show that the crossover disappears for large values of the Majorana overlap energy ξ.

In Fig. 1 we show numerical results obtained for the differential shot noise $\partial S^>(V,V_T)/\partial V$ as a function of the thermal voltage V_T for different values of the bias voltage V. As can be seen, at a certain value of the thermal voltage $V_T = V_{T,\min}$ each of the three curves has a characteristic minimum (shown by the corresponding circle), which represents a crossover from a thermoelectric to pure thermal nonequilibrium behavior. Indeed, the decreasing, or thermoelectric, branch depends on both the electric driving V and thermal driving V_T with the asymptotic behavior shown by the inclined dashed line whereas the increasing, or pure thermal, branch depends only on the thermal driving V_T and does not depend on the electric driving V. Our numerical analysis shows that the asymptotics of the thermoelectric and pure thermal nonequilibrium branches are, respectively, given by the following analytic

expressions:

$$\frac{\partial S^{>}(V,V_T)}{\partial V} = \frac{e^3}{h}\frac{1}{8}\frac{|eV|}{eV_T}, \quad \text{for} \quad V_T: \quad |eV| \ll eV_T \ll eV_{T,\min}, \tag{23}$$

and

$$\frac{\partial S^{>}(V,V_T)}{\partial V} = \frac{e^3}{h}\frac{1-\ln(2)}{4}\frac{\epsilon_d(eV_T)}{\eta^2}, \quad \text{for} \quad V_T: \quad eV_{T,\min} \ll eV_T \ll \Gamma, \tag{24}$$

both of which we are able to reproduce with any desired numerical accuracy. Similarly, in the whole range of the thermal voltage V_T, restricted by the regime specified in Eq. (22), our numerical calculations show that the analytic expression for the differential shot noise is given by the sum of Eqs. (23) and (24),

$$\frac{\partial S^{>}(V,V_T)}{\partial V} = \frac{e^3}{h}\left[\frac{1}{8}\frac{|eV|}{eV_T} + \frac{1-\ln(2)}{4}\frac{\epsilon_d(eV_T)}{|\eta|^2}\right], \quad \text{for} \quad V_T: \quad |eV| \ll eV_T \ll \Gamma. \tag{25}$$

An analytic derivation of Eq. (25) is a complicated task which we would like to address in a separate paper. We note that a proper analytic analysis may provide corrections to Eq. (25) and show under which conditions these corrections start to play an essential role. Also using the Sommerfeld expansion [93], one may analytically derive the differential shot noise in the complementary regime where $eV_T \ll |eV|$. However, within the specified regime, Eq. (22), the analytic expression in Eq. (25) has been confirmed with any desired numerical precision. This means that the stronger the inequalities in Eq. (22) are fulfilled, the more digits after the decimal point are reproduced numerically for any given value obtained analytically from Eq. (25).

From Eq. (25) we find that $eV_{T,\min}$ depends on the bias voltage V, gate voltage ϵ_d and Majorana tunneling amplitude $|\eta|$,

$$eV_{T,\min} = \left\{\frac{1}{2[1-\ln(2)]}\frac{|eV||\eta|^2}{\epsilon_d}\right\}^{\frac{1}{2}}. \tag{26}$$

The differential shot noise at $V_T = V_{T,\min}$ is obtained from Eqs. (25) and (26) which lead to the following result:

$$\left.\frac{\partial S^{>}(V,V_T)}{\partial V}\right|_{V_T=V_{T,\min}} = \frac{e^3}{h}\left[\frac{1-\ln(2)}{8}\frac{\epsilon_d|eV|}{|\eta|^2}\right]^{\frac{1}{2}}. \tag{27}$$

Note, that the thermoelectric branch, Eq. (23), is universal because it does not depend on the gate voltage ϵ_d and depends only on the ratio between the electric and thermal driving, V and V_T, respectively.

According to Eqs. (26) and (27) both the location of the crossover, $V_{T,\min}$, and the value of $\partial S^{>}(V,V_T)/\partial V$ at $V_T = V_{T,\min}$ depend on V. This suggests that the crossover results from an interplay between the electric and thermal driving. Moreover, the dependence of the crossover on ϵ_d in Eqs. (26) and (27) (see also Fig. 2) is another indication that the crossover emerges from a competition of the two flows excited, respectively, by the electric and thermal driving. Obviously, due to the particle-hole symmetry, the current cannot be excited exclusively by the thermal driving V_T when $\epsilon_d = 0$. The pure thermal driving V_T induces a finite current only when $\epsilon_d \neq 0$.

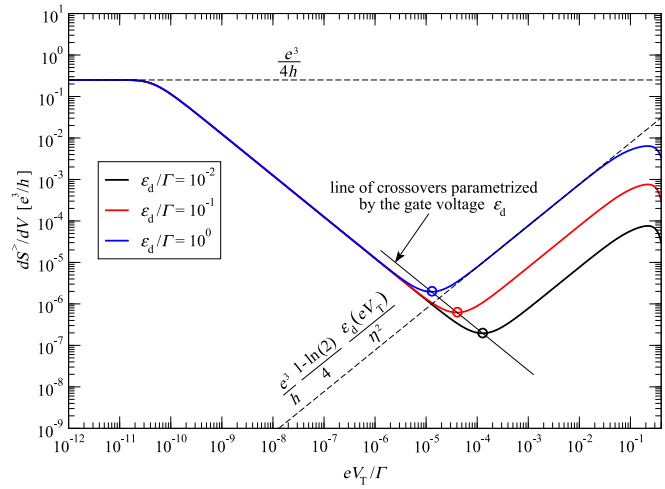

FIG. 2. Differential shot noise $\partial S^{>}/\partial V$ as a function of the thermal voltage V_T for three different values of the gate voltage: $\epsilon_d/\Gamma = 10^{-2}$ (black), $\epsilon_d/\Gamma = 10^{-1}$ (red), $\epsilon_d/\Gamma = 1$ (blue). The other parameters have the following values: $|eV|/\Gamma = 10^{-10}$, $k_BT/\Gamma = 10^{-12}$, $|\eta|/\Gamma = 1$, $\xi/\Gamma = 10^{-14}$.

The straight solid line in Fig. 1 shows both the locations $V_{T,\min}$ of the crossovers and the values of $\partial S^{>}(V,V_T)/\partial V$ at $V_T = V_{T,\min}$ parameterized by the bias voltage V according to Eqs. (26) and (27). The figure clearly shows that the crossovers (highlighted by the circles), obtained from the numerical calculations, reside perfectly on the analytic straight solid line. As expected, at low energies, $eV_T \ll |eV|$ [that is outside the regime in Eq. (22)], the differential shot noise reaches its universal asymptotic unitary value $e^3/4h$ shown by the horizontal dashed line (see also Refs. [54,59]).

The numerical results presented in Fig. 2 show the differential shot noise $\partial S^{>}(V,V_T)/\partial V$ as a function of the thermal voltage V_T for different values of the gate voltage ϵ_d. As in Fig. 1, each of the three curves possesses a crossover (shown by the corresponding circle) from a thermoelectric to pure thermal nonequilibrium behavior. As mentioned above, on the left side of the crossover the decreasing, or thermoelectric, branch is universal: it depends on both the electric driving V and thermal driving V_T via their ratio and Fig. 2 explicitly demonstrates that it does not depend on the gate voltage ϵ_d. On the right side of the crossover the increasing, or pure thermal, branch, which is driven only by the thermal voltage V_T, is obviously not universal. Indeed, the figure clearly shows that this branch depends on the gate voltage ϵ_d. The inclined dashed line shows the asymptotic behavior of the pure thermal nonequilibrium branch, in particular, its dependence on the gate voltage ϵ_d. Note, that in fact this pure thermal nonequilibrium branch is not universal because of two reasons. The first reason, the dependence on ϵ_d, was already mentioned above. The second reason is that this branch additionally depends on the Majorana tunneling amplitude $|\eta|$ as it is also shown in its asymptotic behavior.

In addition to the dependence on V, both the location of the crossover, $V_{T,\min}$, and the value of $\partial S^{>}(V,V_T)/\partial V$ at $V_T = V_{T,\min}$ depend on ϵ_d. The straight solid line shows both the locations $V_{T,\min}$ of the crossovers and the values of $\partial S^{>}(V,V_T)/\partial V$ at $V_T = V_{T,\min}$ parameterized by the gate voltage ϵ_d according to Eqs. (26) and (27). As in the case of the parametric dependence on V, one clearly sees that the numerically obtained crossovers, marked by the circles, also reside perfectly on the analytic straight line resulting from the parametric dependence on ϵ_d. Here the universality of the differential shot noise at low energies, $eV_T \ll |eV|$, is explicitly visible: the asymptotic low-energy behavior is obviously independent of ϵ_d and is characterized by the unitary value $e^3/4h$ shown by the horizontal dashed line.

The nonequilibrium Majorana crossover in the differential shot noise has a number of universal properties which may quantitatively be expressed via a number of ratios taking universal values. For example, according to Eqs. (26) and (27) the ratio

$$R_1 \equiv \frac{eV_{T,\min}}{|eV|}\frac{\partial S^{>}(V,V_T)}{\partial V}\bigg|_{V_T=V_{T,\min}} \tag{28}$$

is independent of V and takes the universal value

$$R_1^{(M)} = \frac{e^3}{4h} \tag{29}$$

for bias voltages satisfying Eq. (22).

For the mean current at low bias voltages in Ref. [41] it has been found that

$$\frac{\partial I(V,V_T)}{\partial V_T} = \frac{e^2}{h}\frac{\pi^2}{12}\frac{\epsilon_d(eV_T)}{|\eta|^2}. \tag{30}$$

Using Eqs. (26), (27), and (30) one finds that the dimensionless ratio

$$R_2 \equiv \frac{\frac{\partial S^{>}(V,V_T)}{\partial V}\big|_{V_T=V_{T,\min}}}{eV_{T,\min}\frac{\partial^2 I(V,V_T)}{\partial V_T^2}} \tag{31}$$

becomes universal,

$$R_2^{(M)} = [1-\ln(2)]\frac{6}{\pi^2} \tag{32}$$

under the conditions in Eq. (22).

If one takes two values of the thermal voltage, V_{T_1} and V_{T_2}, such that V_{T_1} belongs to the thermoelectric branch and V_{T_2} belongs to the pure thermal branch, then from Eqs. (23), (24), and (27) it follows that the dimensionless ratio

$$R_3 \equiv \frac{V_{T_1}}{V_{T_2}}\frac{\frac{\partial S^{>}(V,V_T)}{\partial V}\big|_{V_T=V_{T_1}}\frac{\partial S^{>}(V,V_T)}{\partial V}\big|_{V_T=V_{T_2}}}{\left(\frac{\partial S^{>}(V,V_T)}{\partial V}\big|_{V_T=V_{T,\min}}\right)^2} \tag{33}$$

is universal,

$$R_3^{(M)} = \tfrac{1}{4}, \tag{34}$$

that is independent of V_{T_1} (V_{T_2}) at fixed V_{T_2} (V_{T_1}). This is demonstrated in Fig. 3 where the fixed values of V_{T_1} (lower panel) and V_{T_2} (upper panel) are, respectively, chosen such that $|eV| \ll eV_{T_1} \ll eV_{T,\min}$ and $eV_{T,\min} \ll eV_{T_2} \ll \Gamma$. As one can see in the upper panel of Fig. 3, on the left (thermoelectric)

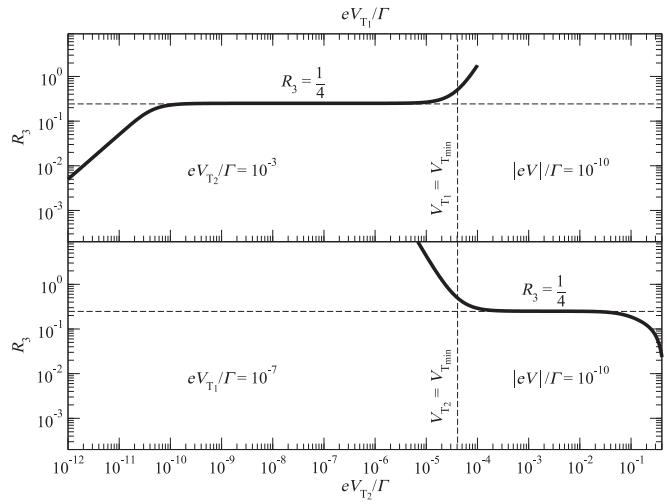

FIG. 3. Dimensionless ratio R_3, defined in Eq. (33), which relates the thermoelectric (V_{T_1} is on the left side of the crossover) and pure thermal (V_{T_2} is on the right side of the crossover) branches of the differential shot noise $\partial S^{>}/\partial V$ via its value at the crossover $V_T = V_{T,\min}$. Upper (Lower) panel: R_3 as a function of V_{T_1} (V_{T_2}) at a fixed value of V_{T_2} (V_{T_1}). Here the values of the parameters are as follows: $\epsilon_d/\Gamma = 10^{-1}$, $|eV|/\Gamma = 10^{-10}$, $k_BT/\Gamma = 10^{-12}$, $|\eta|/\Gamma = 1$, $\xi/\Gamma = 10^{-14}$, and $eV_{T_1}/\Gamma = 10^{-7}$ (lower panel), $eV_{T_2}/\Gamma = 10^{-3}$ (upper panel). For the above values of the parameters one gets from Eq. (26) that $eV_{T,\min}/\Gamma \approx 4\times 10^{-5}$ (see the vertical dashed line).

side of the crossover the numerically obtained dimensionless ratio R_3 has a perfect plateau with $R_3 = 1/4$ (shown by the horizontal dashed line) as expected in the range $|eV| \ll eV_{T_1} \ll eV_{T,\min}$ for any fixed value of V_{T_2} taken from the range $eV_{T,\min} \ll eV_{T_2} \ll \Gamma$. As demonstrated in the lower panel of Fig. 3, also on the right (pure thermal) side of the crossover the numerical curve develops a clear plateau on which $R_3 = 1/4$ (horizontal dashed line) in the range $eV_{T,\min} \ll eV_{T_2} \ll \Gamma$ for any fixed value of V_{T_1} taken from the range $|eV| \ll eV_{T_1} \ll eV_{T,\min}$. In contrast, when V_{T_1} moves away from the thermoelectric branch (left side of the crossover), that is when $eV_{T_1} \lesssim |eV|$ or $V_{T_1} \gtrsim V_{T,\min}$, the ratio R_3 must deviate from the value 1/4. The numerical results (solid curve) in the upper panel show that indeed deviations from the plateau $R_3 = 1/4$ occur when $eV_{T_1} \lesssim |eV|$ or $V_{T_1} \gtrsim V_{T,\min}$. Similarly, when V_{T_2} is not located on the pure thermal branch (right side of the crossover), that is when $V_{T_2} \lesssim V_{T,\min}$ or $eV_{T_2} \gtrsim \Gamma$, the ratio R_3 must also shift away from the plateau on which it reaches the value 1/4. As anticipated, the solid curve resulting from numerical calculations demonstrates that its plateaulike behavior in the lower panel breaks in the domains where $V_{T_2} \lesssim V_{T,\min}$ or $eV_{T_2} \gtrsim \Gamma$.

Now let us consider only the pure thermal nonequilibrium branch of the differential shot noise. From Eqs. (24) and (30) one finds that the ratio

$$R_4 \equiv \frac{\frac{\partial S^{>}(V,V_T)}{\partial V}}{\frac{\partial I(V,V_T)}{\partial V_T}} \tag{35}$$

becomes universal,

$$R_4^{(M)} = e\frac{3[1-\ln(2)]}{\pi^2}, \tag{36}$$

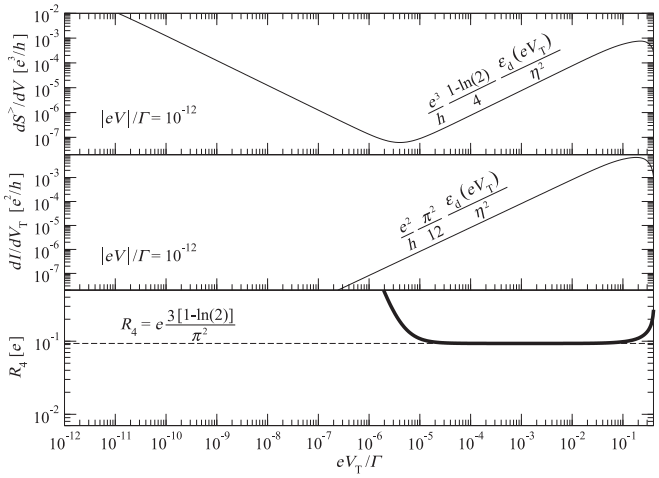

FIG. 4. Differential shot noise $\partial S^{>}/\partial V$ (upper panel), differential thermoelectric conductance $\partial I/\partial V_T$ (middle panel) and their ratio R_4 (lower panel) as functions of the thermal voltage V_T. Here the results have been obtained for the following values of the parameters: $\epsilon_d/\Gamma = 10^{-1}$, $|eV|/\Gamma = 10^{-12}$, $k_BT/\Gamma = 10^{-12}$, $|\eta|/\Gamma = 1$, $\xi/\Gamma = 10^{-14}$. According to Eq. (26), these values of the parameters give $eV_{T,\min}/\Gamma \approx 4 \times 10^{-6}$.

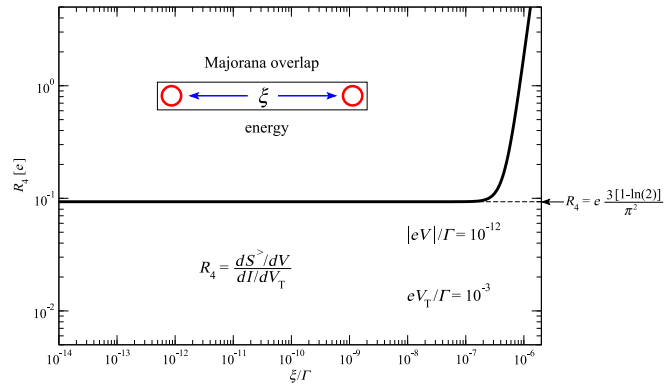

FIG. 5. Ratio R_4 defined in Eq. (35) (duplicated also below the solid curve in the figure) as a function of the Majorana overlap energy ξ. Here we put $\epsilon_d/\Gamma = 10^{-1}$, $|eV|/\Gamma = 10^{-12}$, $eV_T/\Gamma = 10^{-3}$, $k_BT/\Gamma = 10^{-12}$, $|\eta|/\Gamma = 1$.

in the range of the pure thermal nonequilibrium branch. In Fig. 4 we present numerical results for the ratio R_4. From the upper and middle panels one immediately sees the qualitative difference between the behavior of, respectively, the differential shot noise $\partial S^{>}(V, V_T)/\partial V$ and differential thermoelectric conductance $\partial I(V, V_T)/\partial V_T$. Indeed, whereas the differential shot noise $\partial S^{>}(V, V_T)/\partial V$ exhibits in its minimum a crossover separating a thermoelectric branch (left side of the crossover) from a pure thermal branch (right side of the crossover), the differential thermoelectric conductance $\partial I(V, V_T)/\partial V_T$ does not demonstrate any crossover and has only one, pure thermal, nonequilibrium branch. As has been discussed above, in contrast to the universal thermoelectric branch of $\partial S^{>}(V, V_T)/\partial V$, its pure thermal branch is not universal because of its dependence on the gate voltage ϵ_d and the Majorana tunneling amplitude $|\eta|$ as can be seen in Eq. (24). Comparing the two nonuniversal pure thermal branches of the differential shot noise and differential thermoelectric conductance, Eqs. (24) and (30), respectively, one sees that both of them depend linearly on the thermal voltage V_T and have identical parametric dependence on the gate voltage ϵ_d and Majorana tunneling amplitude $|\eta|$. Thus, although the pure thermal branches of the differential shot noise and differential thermoelectric conductance are not universal when considered separately from each other, their ratio R_4 in Eq. (35), must be universal, that is it must be independent of the thermal voltage V_T, gate voltage ϵ_d and Majorana tunneling amplitude $|\eta|$. Moreover, according to Eq. (36), one expects that in the range of V_T corresponding to the pure thermal branch of $\partial S^{>}(V, V_T)/\partial V$ the ratio R_4 must be equal to $3[1 - \ln(2)]/\pi^2$ in the universal units of the elementary charge e. The numerical results presented in the lower panel confirm this expectation: on the right (pure thermal) side of the crossover of $\partial S^{>}(V, V_T)/\partial V$ the ratio R_4 exhibits a plateaulike behavior in the range $eV_{T,\min} \ll eV_T \ll \Gamma$ with $R_4 = 3e[1 - \ln(2)]/\pi^2$ on the plateau. At this point we would also like to note that, similarly to the differential thermoelectric conductance $\partial I(V, V_T)/\partial V_T$, the differential conductance $\partial I(V, V_T)/\partial V$ does not exhibit any crossover. Our numerical calculations show that it remains almost independent of V_T and retains its Majorana fractional value $\partial I(V, V_T)/\partial V = e^2/2h$ up to $eV_T \sim \Gamma$ where it starts to decrease and becomes strongly suppressed, i.e., $\partial I(V, V_T)/\partial V \ll e^2/2h$, for $eV_T \geqslant \Gamma$.

To see what happens when the two MBSs are not well separated, we have performed numerical calculations for larger values of the Majorana overlap energy ξ. Our results show that the above discussed crossover and universal values of the ratios $R_{1,2,3,4}$ disappear. For example, Fig. 5 shows the ratio R_4 as a function of ξ. For well separated MBSs the values of the parameters are chosen to drive the system into the regime where it stays within the plateau shown in the lower panel of Fig. 4, that is when the ratio between the pure thermal branch of the differential shot noise $\partial S^{>}(V, V_T)/\partial V$ and differential thermoelectric conductance $\partial I(V, V_T)/\partial V_T$ takes its universal value, $R_4^{(M)} = 3e[1 - \ln(2)]/\pi^2$. As Fig. 5 clearly demonstrates, for small values of the Majorana overlap energy ξ the ratio between the pure thermal nonequilibrium branches of $\partial S^{>}(V, V_T)/\partial V$ and $\partial I(V, V_T)/\partial V_T$ is equal to its universal Majorana value $R_4^{(M)}$. However, when ξ grows, the two MBSs significantly merge into a single Dirac fermion and cannot be probed separately anymore. In this situation the universal nonequilibrium Majorana behavior breaks. As a consequence, the ratio R_4 significantly deviates from its universal Majorana plateau $R_4^{(M)}$. Moreover, for large values of the Majorana overlap energy ξ both the thermoelectric and pure thermal nonequilibrium branches of the differential shot noise $\partial S^{>}(V, V_T)/\partial V$ are destroyed and the notion of the crossover discussed above loses its sense as one would expect for a phenomenon having a Majorana nature.

Finally, to demonstrate that the universal Majorana thermoelectric crossover in the differential shot noise represents a specific behavior strikingly distinct from what is observed in conventional systems without coupling to MBSs, we have computed $\partial S^{>}(V, V_T)/\partial V$ in the absence of the topological superconductor. The Hamiltonian of the setup without the topological superconductor is obtained from our Hamiltonian if one sets $|\eta| = \xi = 0$. The results obtained for this setup are

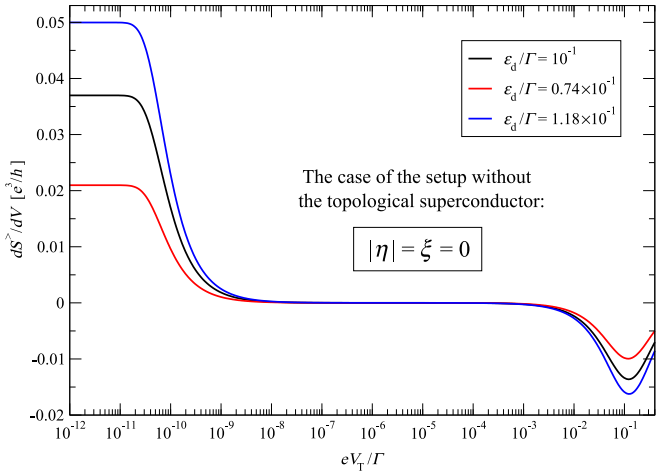

FIG. 6. Differential shot noise $\partial S^>/\partial V$ in the absence of MBSs is shown as a function of the thermal voltage V_T for three different values of the gate voltage: $\epsilon_d/\Gamma = 10^{-1}$ (black), $\epsilon_d/\Gamma = 0.74 \times 10^{-1}$ (red), $\epsilon_d/\Gamma = 1.18 \times 10^{-1}$ (blue). The other parameters have the following values: $|eV|/\Gamma = 10^{-10}$, $k_BT/\Gamma = 10^{-12}$, $|\eta| = \xi = 0$.

shown in Fig. 6. As can be seen, in the absence of MBSs the dependence of the differential shot noise on V_T is qualitatively different from the Majorana induced behavior in two respects.

First, as Fig. 6 shows, the differential shot noise becomes a monotonic function of V_T for $|eV| \ll eV_T \ll \Gamma$. Its monotonically decreasing character makes $\partial S^>(V, V_T)/\partial V$ negative at some point (that is why we avoid using the logarithmic scale for the y axis). In this sense the differential shot noise is not qualitatively singled out because the differential electric and thermoelectric conductances are also monotonically decreasing functions of V_T for $|eV| \ll eV_T \ll \Gamma$ in the absence of MBSs. Specifically, for $|eV| \ll eV_T \ll \Gamma$ the differential electric conductance is almost independent of V_T (and is equal to a value which depends on the gate voltage ϵ_d) up to $eV_T \sim \Gamma$ where it starts to quickly decrease, whereas the differential thermoelectric conductance is, unlike the Majorana case, always negative and decreases linearly with V_T (that is its absolute value grows). In contrast, when MBSs are present, the differential shot noise is qualitatively singled out by its nonmonotonic behavior characterized by a minimum, specifying the thermoelectric crossover, as opposed to the differential electric and thermoelectric conductances having monotonic behavior exhibiting no minima or maxima for $|eV| \ll eV_T \ll \Gamma$.

Second, the three curves in Fig. 6, corresponding to three different values of the gate voltage ϵ_d, demonstrate that in the whole range of the thermal voltage V_T the differential shot noise is not universal, that is, in the absence of MBSs $\partial S^>(V, V_T)/\partial V$ depends on ϵ_d for any value of V_T. This nonuniversal behavior of $\partial S^>(V, V_T)/\partial V$ is qualitatively different from what has been demonstrated in Fig. 2 where coupling to MBSs makes the thermoelectric branch (left side of the crossover) of $\partial S^>(V, V_T)/\partial V$ universal that is independent of ϵ_d. In contrast, without coupling to MBSs even small variations of the gate voltage ϵ_d produce large changes in the differential shot noise $\partial S^>(V, V_T)/\partial V$ in the whole range of the thermal voltage V_T as it is clearly seen in Fig. 6.

IV. CONCLUSION

We have explored the differential shot noise $\partial S^>(V, V_T)/\partial V$ in a Majorana entangled QD device driven out of equilibrium by both the bias voltage V and thermal voltage V_T. The numerical analysis of high precision has been used to reveal the existence of a crossover in the behavior of $\partial S^>(V, V_T)/\partial V$ as a function of V_T and identify its analytic form. In particular, it has been shown that this crossover results from an interplay between the two types of nonequilibrium fluctuations induced by, respectively, V and V_T and separates thermoelectric nonequilibrium behavior of the differential shot noise from its pure thermal nonequilibrium behavior. The energy scale of the crossover as well as its nonequilibrium fluctuation nature invisible for mean current probes have been identified and the crossover dependences on the gate voltage, bias voltage and Majorana tunneling amplitude have been explicitly shown. Additionally, various universal Majorana ratios $R_{1,2,3,4}$ involving the energy scale of the crossover have been provided for a future experimental access to universal fluctuation behavior of Majorana entangled states within either pure noise measurements, ratios $R_{1,3}$, or in combination with measurements of mean currents, ratios $R_{2,4}$. It has been found that the crossover is destroyed when the two MBSs of the topological superconductor start to overlap and merge into a single Dirac fermion. This results in a disappearance of the universal Majorana plateaus in the ratios $R_{1,2,3,4}$ as has been exemplified via numerical calculations for R_4. Finally, we have demonstrated that whereas for Majorana entangled states the differential shot noise has a nonmonotonic behavior characterized by a minimum with universal properties, in conventional systems without coupling to MBSs the differential shot noise is a monotonic and nonuniversal function in the whole range of V_T. Thus, in contrast to Majorana entangled states, in setups without MBSs the monotonic differential shot noise is not qualitatively different from the differential electric and thermoelectric conductances which are also monotonic functions of V_T in the absence of MBSs.

For an experimental verification of the theoretical results presented in this work one might consider the devices studied in Refs. [80,81]. These devices are based on InAs nanowires covered by an Al layer grown by molecular beam epitaxy. The Al layer is the superconductor which is used to induce a topological superconducting state in the InAs nanowire whose ends are assumed to host MBSs $\gamma_{1,2}$. To couple γ_1 to a QD the Al layer is etched on one end of the InAs nanowire. This bare part of InAs is the place where one forms a QD coupled to the Majorana state γ_1 with the coupling strength $|\eta|$. As explained in Ref. [81], the occupancy (or the energy level ϵ_d in our context) of the QD is tuned by proper gate voltages. In addition to the setup in Refs. [80,81], one may also form two independent normal metallic contacts coupled to the QD with the coupling strength Γ. These two independent normal metallic contacts may, in general, have different chemical potentials $\mu_{L,R}$ and different temperatures $T_{L,R}$. To measure the differential shot noise one could try to adapt, for example, the technology from Ref. [92] based on coupling of a setup to a quantum noise detector. Here for the

quantum noise detector one also uses Al as a superconductor and thus it might be compatible with the above technology [80,81] for topological superconductivity. The setup in Ref. [92] is a carbon nanotube. It may be replaced with the InAs nanowire from Refs. [80,81]. One possible problem here is that measurements in Ref. [92] assume finite frequencies. Nevertheless, one may still measure the differential shot noise if the resonant frequencies in Ref. [92] are made smaller than all the relevant energy scales of our setup. This might be achieved, for example, by increasing the length of the transmission lines in Ref. [92] or by other relevant techniques.

Among possible outlooks we would like to mention setups with Aharonov-Bohm fluxes [94] or setups where both MBSs are directly entangled with a QD whose nonequilibrium states are governed by bias voltages and temperature differences. Majorana interference effects in such setups will emerge through the Majorana tunneling phases forming a complex interplay with the two competing flows induced by, respectively, V and V_T and the fate of the Majorana crossover in $\partial S^{>}(V, V_T)/\partial V$ in this situation is an interesting and important problem. The results presented in this work have been obtained assuming that interactions between the Majorana entangled setup and its environment are sufficiently weak. Under certain circumstances, however, such interactions may have a significant impact on the shot noise via corresponding inelastic processes [95] and thus represent a challenge for future models where MBSs are coupled to an external environment. Another possibility is to study the differential shot noise in nonequilibrium setups with poor man's MBSs [96,97] which may arise inside QDs when one fine-tunes parameters of such setups to locate their states as close as possible to their sweet spots.

ACKNOWLEDGMENT

The author thanks R. Egger for valuable comments.

[1] A. Yu. Kitaev, Unpaired Majorana fermions in quantum wires, Phys. Usp. **44**, 131 (2001).
[2] J. Alicea, New directions in the pursuit of Majorana fermions in solid state systems, Rep. Prog. Phys. **75**, 076501 (2012).
[3] M. Leijnse and K. Flensberg, Introduction to topological superconductivity and Majorana fermions, Semicond. Sci. Technol. **27**, 124003 (2012).
[4] M. Sato and S. Fujimoto, Majorana fermions and topology in superconductors, J. Phys. Soc. Jpn. **85**, 072001 (2016).
[5] R. Aguado, Majorana quasiparticles in condensed matter, La Riv. del Nuovo Cimento **40**, 523 (2017).
[6] R. M. Lutchyn, E. P. A. M. Bakkers, L. P. Kouwenhoven, P. Krogstrup, C. M. Marcus, and Y. Oreg, Majorana zero modes in superconductor-semiconductor heterostructures, Nat. Rev. Mater. **3**, 52 (2018).
[7] V. V. Val'kov, M. S. Shustin, S. V. Aksenov, A. O. Zlotnikov, A. D. Fedoseev, V. A. Mitskan, and M. Yu. Kagan, Topological superconductivity and Majorana states in low-dimensional systems, Phys. Usp. **65**, 2 (2022).
[8] E. Majorana, Teoria simmetrica dell'elettrone e del positrone, Nuovo Cimento **14**, 171 (1937).
[9] A. Yu. Kitaev, Fault-tolerant quantum computation by anyons, Ann. Phys. **303**, 2 (2003).
[10] D. E. Liu and H. U. Baranger, Detecting a Majorana-fermion zero mode using a quantum dot, Phys. Rev. B **84**, 201308(R) (2011).
[11] L. Fidkowski, J. Alicea, N. H. Lindner, R. M. Lutchyn, and M. P. A. Fisher, Universal transport signatures of Majorana fermions in superconductor-Luttinger liquid junctions, Phys. Rev. B **85**, 245121 (2012).
[12] E. Prada, P. San-Jose, and R. Aguado, Transport spectroscopy of *NS* nanowire junctions with Majorana fermions, Phys. Rev. B **86**, 180503(R) (2012).
[13] F. Pientka, G. Kells, A. Romito, P. W. Brouwer, and F. von Oppen, Enhanced Zero-Bias Majorana Peak in the Differential Tunneling Conductance of Disordered Multisubband Quantum-Wire/Superconductor Junctions, Phys. Rev. Lett. **109**, 227006 (2012).
[14] C.-H. Lin, J. D. Sau, and S. Das Sarma, Zero-bias conductance peak in Majorana wires made of semiconductor/superconductor hybrid structures, Phys. Rev. B **86**, 224511 (2012).
[15] M. Lee, J. S. Lim, and R. López, Kondo effect in a quantum dot side-coupled to a topological superconductor, Phys. Rev. B **87**, 241402(R) (2013).
[16] A. Kundu and B. Seradjeh, Transport Signatures of Floquet Majorana Fermions in Driven Topological Superconductors, Phys. Rev. Lett. **111**, 136402 (2013).
[17] E. Vernek, P. H. Penteado, A. C. Seridonio, and J. C. Egues, Subtle leakage of a Majorana mode into a quantum dot, Phys. Rev. B **89**, 165314 (2014).
[18] R. Ilan, J. H. Bardarson, H.-S. Sim, and J. E. Moore, Detecting perfect transmission in Josephson junctions on the surface of three dimensional topological insulators, New J. Phys. **16**, 053007 (2014).
[19] M. Cheng, M. Becker, B. Bauer, and R. M. Lutchyn, Interplay between Kondo and Majorana Interactions in Quantum Dots, Phys. Rev. X **4**, 031051 (2014).
[20] A. M. Lobos and S. Das Sarma, Tunneling transport in NSN Majorana junctions across the topological quantum phase transition, New J. Phys. **17**, 065010 (2015).
[21] Y. Peng, F. Pientka, Y. Vinkler-Aviv, L. I. Glazman, and F. von Oppen, Robust Majorana Conductance Peaks for a Superconducting Lead, Phys. Rev. Lett. **115**, 266804 (2015).
[22] G. Sharma and S. Tewari, Tunneling conductance for Majorana fermions in spin-orbit coupled semiconductor-superconductor heterostructures using superconducting leads, Phys. Rev. B **93**, 195161 (2016).
[23] B. van Heck, R. M. Lutchyn, and L. I. Glazman, Conductance of a proximitized nanowire in the Coulomb blockade regime, Phys. Rev. B **93**, 235431 (2016).
[24] S. Das Sarma, A. Nag, and J. D. Sau, How to infer non-Abelian statistics and topological visibility from tunneling conductance

properties of realistic Majorana nanowires, Phys. Rev. B **94**, 035143 (2016).

[25] R. M. Lutchyn and L. I. Glazman, Transport through a Majorana Island in the Strong Tunneling Regime, Phys. Rev. Lett. **119**, 057002 (2017).

[26] C.-X. Liu, J. D. Sau, T. D. Stanescu, and S. Das Sarma, Andreev bound states versus Majorana bound states in quantum dot-nanowire-superconductor hybrid structures: Trivial versus topological zero-bias conductance peaks, Phys. Rev. B **96**, 075161 (2017).

[27] H. Huang, Q.-F. Liang, D.-X. Yao, and Z. Wang, Majorana ϕ_0-junction in a disordered spin-orbit coupling nanowire with tilted magnetic field, Physica C **543**, 22 (2017).

[28] C.-X. Liu, J. D. Sau, and S. Das Sarma, Distinguishing topological Majorana bound states from trivial Andreev bound states: Proposed tests through differential tunneling conductance spectroscopy, Phys. Rev. B **97**, 214502 (2018).

[29] Y.-H. Lai, J. D. Sau, and S. Das Sarma, Presence versus absence of end-to-end nonlocal conductance correlations in Majorana nanowires: Majorana bound states versus Andreev bound states, Phys. Rev. B **100**, 045302 (2019).

[30] L.-W. Tang and W.-G. Mao, Detection of Majorana bound states by sign change of the tunnel magnetoresistance in a quantum dot coupled to ferromagnetic electrodes, Front. Phys. **8**, 147 (2020).

[31] G. Zhang and C. Spånslätt, Distinguishing between topological and quasi Majorana zero modes with a dissipative resonant level, Phys. Rev. B **102**, 045111 (2020).

[32] F. Chi, T.-Y. He, and G. Zhou, Photon-assisted average current through a quantum dot coupled to Majorana bound states, J. Nanoelectron. Optoelectron. **16**, 1325 (2021).

[33] Z.-H. Wang and W.-C. Huang, Dual negative differential of heat generation in a strongly correlated quantum dot side-coupled to Majorana bound states, Front. Phys. **9**, 727934 (2021).

[34] T. H. Galambos, F. Ronetti, B. Hetényi, D. Loss, and J. Klinovaja, Crossed Andreev reflection in spin-polarized chiral edge states due to the Meissner effect, Phys. Rev. B **106**, 075410 (2022).

[35] J. Jin and X.-Q. Li, Master equation approach for transport through Majorana zero modes, New J. Phys. **24**, 093009 (2022).

[36] W.-K. Zou, N.-W. Li, and F.-L. Chong, Charge and spin transports through a normal lead coupled to an s-wave superconductor and Majorana fermions, Phys. Status Solidi B, 2200472 (2023).

[37] M. Leijnse, Thermoelectric signatures of a Majorana bound state coupled to a quantum dot, New J. Phys. **16**, 015029 (2014).

[38] R. López, M. Lee, L. Serra, and J. S. Lim, Thermoelectrical detection of Majorana states, Phys. Rev. B **89**, 205418 (2014).

[39] H. Khim, R. López, J. S. Lim, and M. Lee, Thermoelectric effect in the Kondo dot side-coupled to a Majorana mode, Eur. Phys. J. B **88**, 151 (2015).

[40] J. P. Ramos-Andrade, O. Ávalos-Ovando, P. A. Orellana, and S. E. Ulloa, Thermoelectric transport through Majorana bound states and violation of Wiedemann-Franz law, Phys. Rev. B **94**, 155436 (2016).

[41] S. Smirnov, Dual Majorana universality in thermally induced nonequilibrium, Phys. Rev. B **101**, 125417 (2020).

[42] T.-Y. He, H. Sun, and G. Zhou, Photon-assisted Seebeck effect in a quantum dot coupled to Majorana zero modes, Front. Phys. **9**, 687438 (2021).

[43] D. Giuliano, A. Nava, R. Egger, P. Sodano, and F. Buccheri, Multiparticle scattering and breakdown of the Wiedemann-Franz law at a junction of N interacting quantum wires, Phys. Rev. B **105**, 035419 (2022).

[44] F. Buccheri, A. Nava, R. Egger, P. Sodano, and D. Giuliano, Violation of the Wiedemann-Franz law in the topological Kondo model, Phys. Rev. B **105**, L081403 (2022).

[45] P. Majek, K. P. Wójcik, and I. Weymann, Spin-resolved thermal signatures of Majorana-Kondo interplay in double quantum dots, Phys. Rev. B **105**, 075418 (2022).

[46] N. Bondyopadhaya and D. Roy, Nonequilibrium electrical, thermal and spin transport in open quantum systems of topological superconductors, semiconductors and metals, J. Stat. Phys. **187**, 11 (2022).

[47] W.-K. Zou, Q. Wang, and H.-K. Zhao, Aharonov-Bohm oscillations in the Majorana fermion modulated charge and heat transports through a double-quantum-dot interferometer, Phys. Lett. A **443**, 128219 (2022).

[48] V. Mourik, K. Zuo, S. M. Frolov, S. R. Plissard, E. P. A. M. Bakkers, and L. P. Kouwenhoven, Signatures of Majorana fermions in hybrid superconductor-semiconductor nanowire devices, Science **336**, 1003 (2012).

[49] S. Nadj-Perge, I. K. Drozdov, J. Li, H. Chen, S. Jeon, J. Seo, A. H. MacDonald, B. A. Bernevig, and A. Yazdani, Observation of Majorana fermions in ferromagnetic atomic chains on a superconductor, Science **346**, 602 (2014).

[50] Z. Wang, H. Song, D. Pan, Z. Zhang, W. Miao, R. Li, Z. Cao, G. Zhang, L. Liu, L. Wen, R. Zhuo, D. E. Liu, K. He, R. Shang, J. Zhao, and H. Zhang, Plateau Regions for Zero-Bias Peaks within 5% of the Quantized Conductance Value $2e^2/h$, Phys. Rev. Lett. **129**, 167702 (2022).

[51] P. Yu, J. Chen, M. Gomanko, G. Badawy, E. P. A. M. Bakkers, K. Zuo, V. Mourik, and S. M. Frolov, Non-Majorana states yield nearly quantized conductance in proximatized nanowires, Nat. Phys. **17**, 482 (2021).

[52] S. Frolov, Quantum computing's reproducibility crisis: Majorana fermions, Nature (London) **592**, 350 (2021).

[53] A. Ziesen, A. Altland, R. Egger, and F. Hassler, Statistical Majorana Bound State Spectroscopy, Phys. Rev. Lett. **130**, 106001 (2023).

[54] D. E. Liu, M. Cheng, and R. M. Lutchyn, Probing Majorana physics in quantum-dot shot-noise experiments, Phys. Rev. B **91**, 081405(R) (2015).

[55] D. E. Liu, A. Levchenko, and R. M. Lutchyn, Majorana zero modes choose Euler numbers as revealed by full counting statistics, Phys. Rev. B **92**, 205422 (2015).

[56] A. Haim, E. Berg, F. von Oppen, and Y. Oreg, Current correlations in a Majorana beam splitter, Phys. Rev. B **92**, 245112 (2015).

[57] S. Valentini, M. Governale, R. Fazio, and F. Taddei, Finite-frequency noise in a topological superconducting wire, Physica E **75**, 15 (2016).

[58] A. Zazunov, R. Egger, and A. Levy Yeyati, Low-energy theory of transport in Majorana wire junctions, Phys. Rev. B **94**, 014502 (2016).

[59] S. Smirnov, Non-equilibrium Majorana fluctuations, New J. Phys. **19**, 063020 (2017).

[60] T. Jonckheere, J. Rech, A. Zazunov, R. Egger, A. L. Yeyati, and T. Martin, Giant Shot Noise from Majorana Zero Modes in Topological Trijunctions, Phys. Rev. Lett. **122**, 097003 (2019).

[61] S. Smirnov, Majorana finite-frequency nonequilibrium quantum noise, Phys. Rev. B **99**, 165427 (2019).

[62] J. Manousakis, C. Wille, A. Altland, R. Egger, K. Flensberg, and F. Hassler, Weak Measurement Protocols for Majorana Bound State Identification, Phys. Rev. Lett. **124**, 096801 (2020).

[63] G.-H. Feng and H.-H. Zhang, Probing robust Majorana signatures by crossed Andreev reflection with a quantum dot, Phys. Rev. B **105**, 035148 (2022).

[64] S. Smirnov, Revealing universal Majorana fractionalization using differential shot noise and conductance in nonequilibrium states controlled by tunneling phases, Phys. Rev. B **105**, 205430 (2022).

[65] S. Smirnov, Majorana tunneling entropy, Phys. Rev. B **92**, 195312 (2015).

[66] E. Sela, Y. Oreg, S. Plugge, N. Hartman, S. Lüscher, and J. Folk, Detecting the Universal Fractional Entropy of Majorana Zero Modes, Phys. Rev. Lett. **123**, 147702 (2019).

[67] S. Smirnov, Majorana entropy revival via tunneling phases, Phys. Rev. B **103**, 075440 (2021).

[68] S. Smirnov, Majorana ensembles with fractional entropy and conductance in nanoscopic systems, Phys. Rev. B **104**, 205406 (2021).

[69] M. Tanhayi Ahari, S. Zhang, J. Zou, and Y. Tserkovnyak, Biasing topological charge injection in topological matter, Phys. Rev. B **104**, L201401 (2021).

[70] N. Hartman, C. Olsen, S. Lüscher, M. Samani, S. Fallahi, G. C. Gardner, M. Manfra, and J. Folk, Direct entropy measurement in a mesoscopic quantum system, Nat. Phys. **14**, 1083 (2018).

[71] Y. Kleeorin, H. Thierschmann, H. Buhmann, A. Georges, L. W. Molenkamp, and Y. Meir, How to measure the entropy of a mesoscopic system via thermoelectric transport, Nat. Commun. **10**, 5801 (2019).

[72] E. Pyurbeeva and J. A. Mol, A thermodynamic approach to measuring entropy in a few-electron nanodevice, Entropy **23**, 640 (2021).

[73] T. Child, O. Sheekey, S. Lüscher, S. Fallahi, G. C. Gardner, M. Manfra, and J. Folk, A robust protocol for entropy measurement in mesoscopic circuits, Entropy **24**, 417 (2022).

[74] C. Han, Z. Iftikhar, Y. Kleeorin, A. Anthore, F. Pierre, Y. Meir, A. K. Mitchell, and E. Sela, Fractional Entropy of Multichannel Kondo Systems from Conductance-Charge Relations, Phys. Rev. Lett. **128**, 146803 (2022).

[75] E. Pyurbeeva, J. A. Mol, and P. Gehring, Electronic measurements of entropy in meso- and nanoscale systems, Chem. Phys. Rev. **3**, 041308 (2022).

[76] T. Child, O. Sheekey, S. Lüscher, S. Fallahi, G. C. Gardner, M. Manfra, A. Mitchell, E. Sela, Y. Kleeorin, Y. Meir, and J. Folk, Entropy Measurement of a Strongly Coupled Quantum Dot, Phys. Rev. Lett. **129**, 227702 (2022).

[77] S. Smirnov, Universal Majorana thermoelectric noise, Phys. Rev. B **97**, 165434 (2018).

[78] S. Smirnov, Dynamic Majorana resonances and universal symmetry of nonequilibrium thermoelectric quantum noise, Phys. Rev. B **100**, 245410 (2019).

[79] Z. Cao, G. Zhang, H. Zhang, Y.-X. Liang, W.-X. He, K. He, and D. E. Liu, Towards strong evidence of Majorana bound state by a combined measurement of tunneling conductance and current noise, arXiv:2301.06451v1.

[80] M. T. Deng, S. Vaitiekėnas, E. B. Hansen, J. Danon, M. Leijnse, K. Flensberg, J. Nygård, P. Krogstrup, and C. M. Marcus, Majorana bound state in a coupled quantum-dot hybrid-nanowire system, Science **354**, 1557 (2016).

[81] M.-T. Deng, S. Vaitiekėnas, E. Prada, P. San-Jose, J. Nygård, P. Krogstrup, R. Aguado, and C. M. Marcus, Nonlocality of Majorana modes in hybrid nanowires, Phys. Rev. B **98**, 085125 (2018).

[82] D. C. Ralph and R. A. Buhrman, Kondo-assisted and Resonant Tunneling via a Single Charge Trap: A Realization of the Anderson Model Out of Equilibrium, Phys. Rev. Lett. **72**, 3401 (1994).

[83] D. Goldhaber-Gordon, H. Shtrikman, D. Mahalu, D. Abusch-Magder, U. Meirav, and M. A. Kastner, Kondo effect in a single-electron transistor, Nature (London) **391**, 156 (1998).

[84] Y. Meir, N. S. Wingreen, and P. A. Lee, Low-temperature Transport Through a Quantum Dot: The Anderson Model out of Equilibrium, Phys. Rev. Lett. **70**, 2601 (1993).

[85] N. S. Wingreen and Y. Meir, Anderson model out of equilibrium: Noncrossing-approximation approach to transport through a quantum dot, Phys. Rev. B **49**, 11040 (1994).

[86] S. Smirnov and M. Grifoni, Slave-boson Keldysh field theory for the Kondo effect in quantum dots, Phys. Rev. B **84**, 125303 (2011).

[87] S. Smirnov and M. Grifoni, Kondo effect in interacting nanoscopic systems: Keldysh field integral theory, Phys. Rev. B **84**, 235314 (2011).

[88] M. Niklas, S. Smirnov, D. Mantelli, M. Margańska, N.-V. Nguyen, W. Wernsdorfer, J.-P. Cleuziou, and M. Grifoni, Blocking transport resonances via Kondo many-body entanglement in quantum dots, Nat. Commun. **7**, 12442 (2016).

[89] D. A. Ruiz-Tijerina, E. Vernek, L. G. G. V. Dias da Silva, and J. C. Egues, Interaction effects on a Majorana zero mode leaking into a quantum dot, Phys. Rev. B **91**, 115435 (2015).

[90] A. Altland and B. Simons, *Condensed Matter Field Theory*, 2nd ed. (Cambridge University Press, Cambridge, 2010).

[91] Y. Xu, J. Jin, S. Wang, and Y. J. Yan, Memory-effect-preserving quantum master equation approach to noise spectrum of transport current, Phys. Rev. E **106**, 064130 (2022).

[92] J. Basset, A. Y. Kasumov, C. P. Moca, G. Zaránd, P. Simon, H. Bouchiat, and R. Deblock, Measurement of Quantum Noise in a Carbon Nanotube Quantum Dot in the Kondo Regime, Phys. Rev. Lett. **108**, 046802 (2012).

[93] N. W. Ashkroft and N. D. Mermin, *Solid State Physics* (Saunders College, Philadelphia, 1976).

[94] W.-K. Zou, Q. Wang, and H.-K. Zhao, Dynamic heat and charge transports through double-quantum-dot-interferometer modulated by Majorana bound states and time-oscillating Aharonov-Bohm flux, J. Phys.: Condens. Matter **35**, 165303 (2023).

[95] I. V. Krainov, A. P. Dmitriev, and N. S. Averkiev, Shot noise in resonant tunneling: Role of inelastic scattering, Phys. Rev. B **106**, 245421 (2022).

[96] A. Tsintzis, R. S. Souto, and M. Leijnse, Creating and detecting poor man's Majorana bound states in interacting quantum dots, Phys. Rev. B **106**, L201404 (2022).

[97] T. Dvir, G. Wang, N. van Loo, C.-X. Liu, G. P. Mazur, A. Bordin, S. L. D. ten Haaf, J.-Y. Wang, D. van Driel, F. Zatelli, X. Li, F. K. Malinowski, S. Gazibegovic, G. Badawy, E. P. A. M. Bakkers, M. Wimmer, and L. P. Kouwenhoven, Realization of a minimal Kitaev chain in coupled quantum dots, Nature **614**, 445 (2023).